Original article

Compact planar phased array antenna for extended V2X communication coverage

Ye-Bon Kim [a], Han Lim Lee [a,b,*]

[a] School of Electrical and Electronics Engineering, Chung-Ang University, Seoul 06974, South Korea
[b] Department of Intelligent Semiconductor Engineering, Chung-Ang University, Seoul 06974, South Korea

A B S T R A C T

In this article, a new compact planar phased array antenna is proposed for blind spot reduction in V2X communications. The proposed antenna can be easily integrated on the front-panel or rear-view side by providing 2-dimensional wide communication coverage while overcoming physical integration space limitations. Moreover, because the proposed antenna is based on a planar structure, it can be integrated effectively with beamforming circuits. To verify the proposed antenna, both single and array configurations were fabricated and compared with conventional patch antennas at 5.9 GHz. The proposed single antenna with a size of $1\lambda_0 \times 1.1\lambda_0 \times 0.02\lambda_0$ exhibited a measured bandwidth of 4.3% and a peak gain of 6.1 dBi. The measured HPBWs in the E- and H-planes were approximately 126° and 136°, respectively, compared to 75.5° and 66.9° for the conventional patch antenna. Further, the proposed antenna and reference patch antenna were extended to 1×8 array configurations with 8-ch beamforming circuits. The measured scan angle of the proposed antenna was 160°, compared to only 98° for the patch antenna. Finally, a vehicular communication test was conducted with 256-QAM signals, where the proposed 1×8 antenna array exhibited a stable error vector magnitude (EVM) over a wide coverage angle of 150°.

1. Introduction

The increasing interest in fully autonomous driving has resulted in the development of wireless vehicular communication with high speed, low latency, and high data rates. Vehicle-to-everything (V2X) is an essential technology for autonomous driving that has been conducted with dedicated short-range communication (DSRC) and cooperative intelligent transport systems (C-ITSs). IEEE identified the 802.11p/ WAVE standard for V2X communication, with an allocation of 5.850–5.925 GHz [1–3]. Furthermore, studies are being conducted on various scenarios such as line-of-sight (LOS) and non-line-of-sight (NLOS) environments [4–6]. Since the physical mounting positions of the sensor and communication antenna module are limited due to the vehicle characteristics [7–12], it is important to secure communication coverage to ensure that blind spots do not occur while the number of necessary parts is minimized as described in Fig. 1.

The conventional patch antennas for vehicular communication are generally mounted in the vehicle's front or rear areas, resulting in a blind spot for V2X applications. Thus, to overcome the limited HPBW performance of planar-type patch antennas, various research has been conducted on antennas with wide beamwidth characteristics. For example, electrically small planar Huygens source antennas have been proposed [13–18]. However, these antennas have a complicated geometry and are low gain with a very narrow impedance bandwidth. Other approaches based on metasurface, or dielectric resonator antennas have also been proposed [19–24]. However, these require additional metal walls and complex geometry to achieve wide HPBW, rendering them unsuitable for V2X applications in-vehicle. To meet the requirements of compact size and high gain, antennas using a half-mode substrate integrated waveguide (HMSIW) have been reported [25–30]. However, their HPBW performance is too narrow, meaning they are also unsuitable for use as V2X communication antennas mounted in vehicles. From a comprehensive perspective, antennas such as magnetic dipole or multipole types are considered excellent candidates, as they provide wide beam coverage in a limited space [31–37]. However, no research has been conducted on the actual beam coverage by sending and receiving data from wireless communication devices within a size that can be fitted into an actual vehicle. In-vehicle mounted V2X beamforming antennas need to be compact with wide beam coverage and high gain. Thus, to overcome the limited performance of the previously
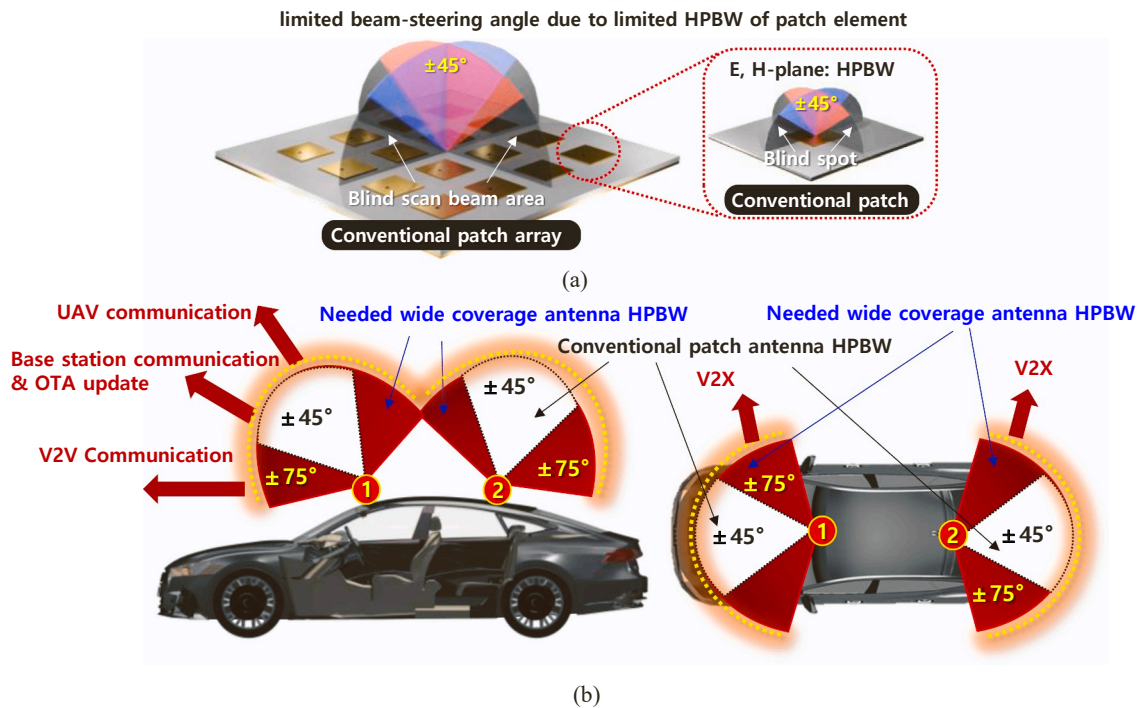
Fig. 1. V2X compact antenna: (a) Conventional planar patch antenna in V2X beamforming applications with limited half-power beamwidth (HPBW) characteristics and (b) in-vehicle mounting position of the proposed antenna with extended communication coverages.
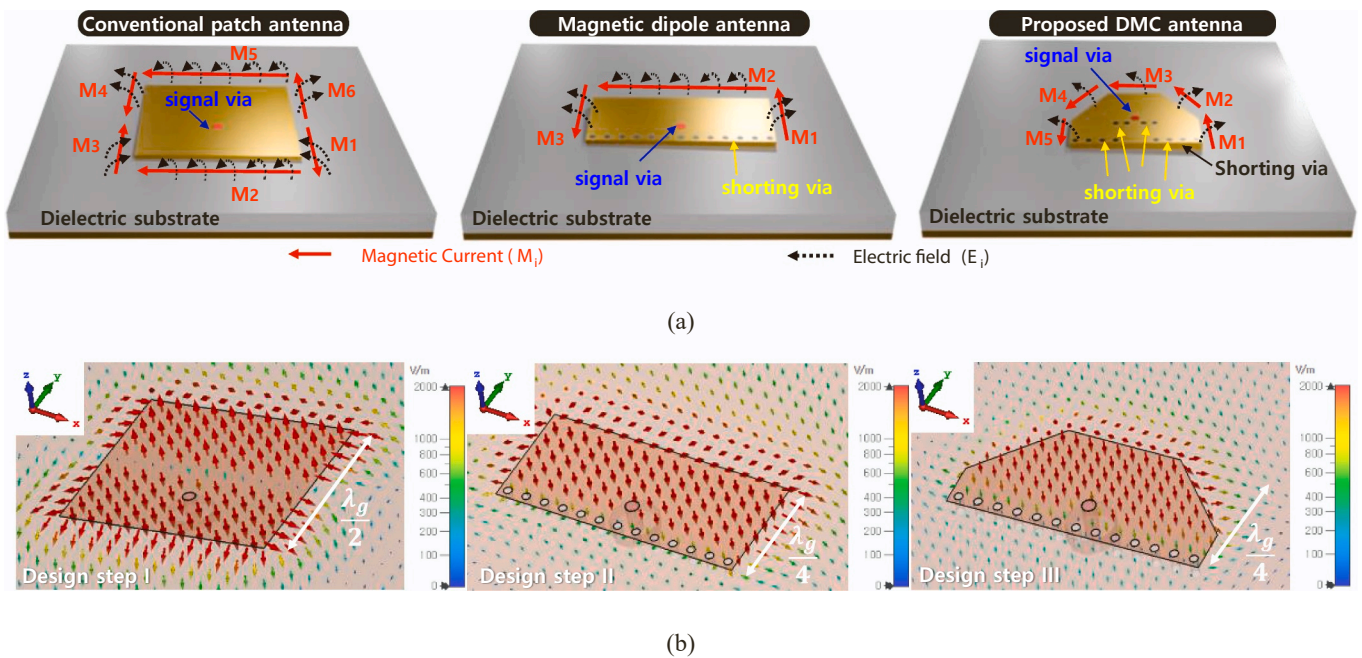

Fig. 2. Planar antenna structures with (a) representative radiating edges and (b) 3-D EM simulated electric field comparisons of the antennas.

studied antennas, a new compact planar structure with wide communication coverage for V2X antenna for in-vehicle mounting in front or rear areas is proposed in this paper.

2. Design and analysis of the proposed antenna

Fig. 2 displays an analysis of the electromagnetic (EM) field radiation by a reference patch antenna, a reference magnetic dipole (MD) antenna, and the proposed diverse magnetic current (DMC) antenna. In this article, all 3-D EM simulations have been conducted using the CST

Studio Suite tool. First, the radiation source can be represented by magnetic currents, which are induced around radiator edges. According to the well-known EM theory, the equivalent magnetic current at each radiating edge can be expressed as

$$\vec{M}_i = -\vec{a}_n \times \vec{E}_i, \tag{1}$$

where a_n is the normal vector, and E_i is the tangential electric field intensity at the radiating edges while M_i is the magnetic current representation at the corresponding radiating edge denoted by i.
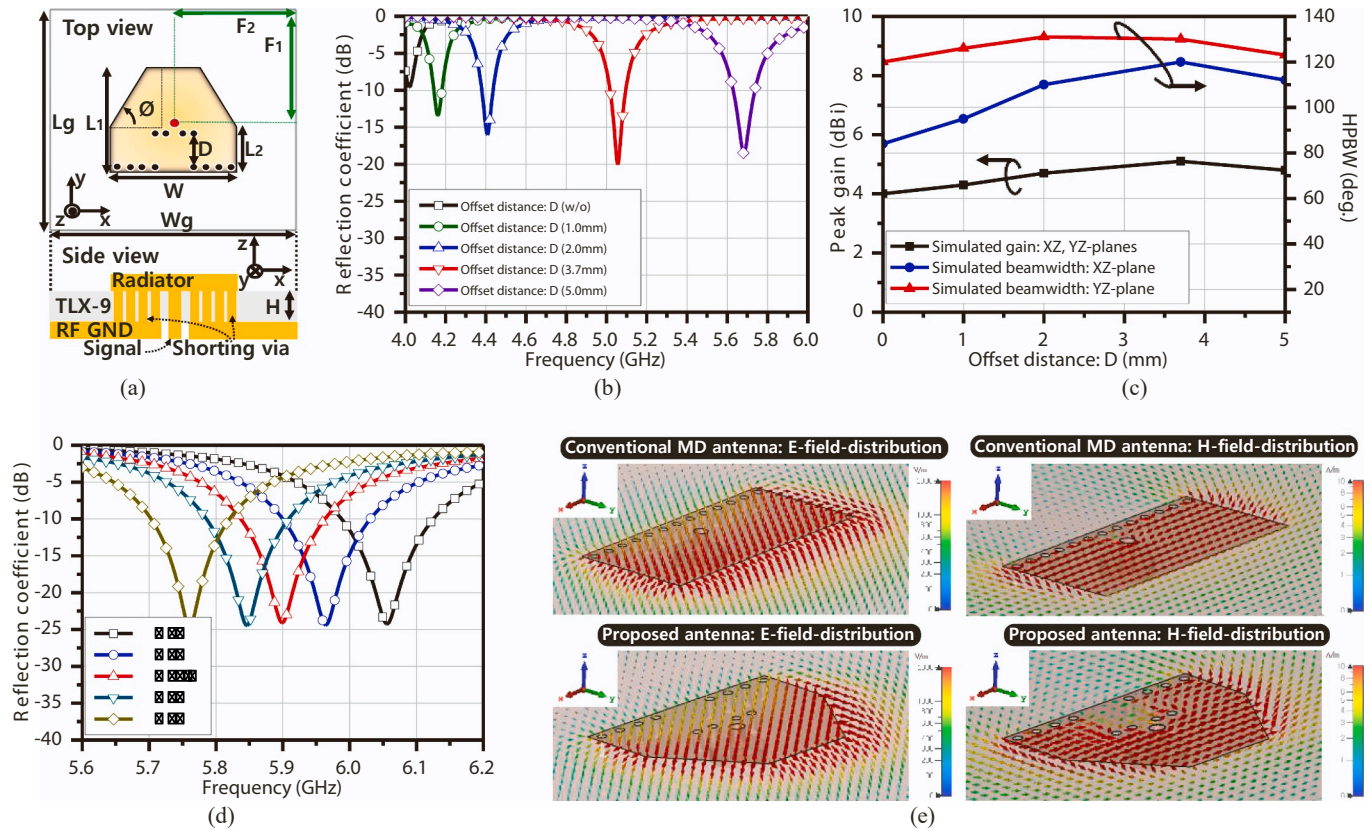
Fig. 3. Proposed DMC antenna structure with (a) geometric parameters, simulated results of reflection coefficient according to (b) D and (c) ϕ, (c) 2-D HPBW optimization according to D at 5.9 GHz.

In the case of a conventional patch antenna, the radiation is weakened because M1, M6 and M3, M4 cancel each other, meaning that only M2 and M5 contribute to the beam radiation pattern as shown in Fig. 2 (a). This results in a limited half-power beamwidth. Therefore, to increase the beamwidth, magnetic dipole antennas have been widely researched. In the case of a commonly used magnetic dipole antenna, one end of an antenna radiator (to which a signal is applied) is connected to ground through a shorting via, as displayed in Fig. 2(a). This means that at the locations of the aligned vias, the electric field strength is zero. Hence, M2 becomes the dominant source and forms a radiation beam pattern by equivalence modeling theory. However, in existing magnetic dipole antenna structures, a surface current is induced in one direction according to the direction of the vias aligned in a row, forming a wide beamwidth in one direction only due to M1 and M3 having relatively weak intensities. Given these considerations, we propose a new compact antenna structure with wide beamwidth characteristics in all directions that uses the concept of a conventional magnetic dipole antenna. Unlike the conventional MD antenna method, the proposed DMC antenna structure is designed such that it changes the direction of the surface current by placing an offset shorting via between a feeding part and an end ground via without aligning the ground vias on the same line. Finally, the proposed antenna is optimized by using a non-square-plane radiator to regulate the electrical length of the surface current flowing

along the outer periphery of the antenna, reducing the size of the radiator by varying the current flow. Simultaneously, M1–M5 are formed on all the outer sides of the radiator, making it possible to create an antenna with a 2-D wide beamwidth, as displayed in Fig. 2(a). The representative models are 3-D EM simulated as shown in Fig. 2(b), where the electric fields along the radiating edges are demonstrated.

To verify the wide beamwidth of the proposed antenna structure at 5.9 GHz, the DMC antenna has been designed following the process described in Fig. 3(a). Moreover, to demonstrate the feasibility of the DMC antenna, a patch antenna, an MD antenna, and the proposed antenna has been analyzed using the same substrate and overall antenna size. All the antennas have been designed using a Taconic TLX-9 substrate with a relative permittivity of 2.5 and a thickness of 1.1 mm. In addition, a typical finite ground size of $1.0 \lambda_0 \times 1.1 \lambda_0$ has been applied. Next, the proposed DMC antenna has been designed by adjusting the offset vias and signal feeder from the square radiator of a reference MD antenna. Fig. 3(b) and (c) display the parametric analysis of the reflection coefficient based on the offset shorting via by D and the angle of the radiator by ϕ, respectively. First, the proposed antenna has been optimized according to the results of the reflection coefficient, antenna gain, and beamwidth variation with respect to the offset via distance, where a D value of 3.7 mm has been found to be the most efficient. In addition, by designing the square side of the radiator with multiple angles while

Table 1
Geometric parameters for the reference patch, reference magnetic dipole, and proposed dmc antennas.

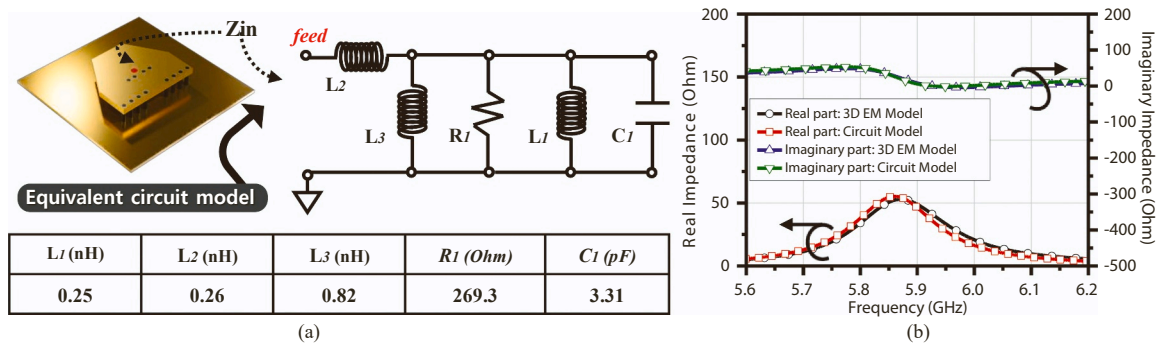| Type	Parameters (mm)									
	Wg	Lg	H	W	L1	L2	D	F1	F2	ϕ
Reference patch	55	60	1.1	16	14.8	0	0	32.9	27.5	0
Reference MD	55	60	1.1	18	7.8	0	0	31.4	27.5	0
Proposed DMC	55	60	1.1	13.8	5.2	6.4	3.7	30.4	27.5	58.5

Fig. 4. Proposed DMC antenna with (a) equivalent circuit model and (b) simulated impedance parameters by 3-D EM and circuit models.
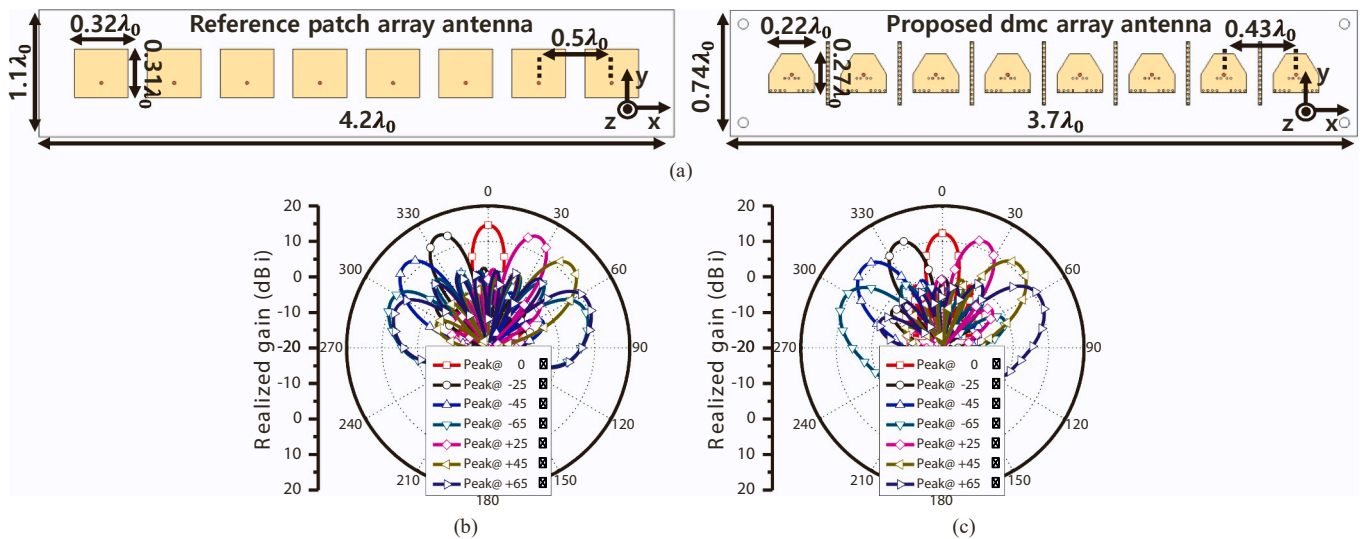

Fig. 5. (a) 1 × 8 array antenna structures and simulated radiation patterns of the array, (b) reference patch, and (c) proposed DMC antenna in xz plane at 5.9 GHz.

fixing the offset via distance, we analyzed the reflection coefficient according to the angle and tuned it to the desired resonant frequency of 5.9 GHz, as displayed in Fig. 3(d). The beamwidth could be increased through a field analysis of the flow of magnetic fields and currents in different directions of the final designed proposed DMC antenna, as depicted in Fig. 3(e). The optimized performance for each antenna will be presented with both simulation and measurement in section III. Finally, the configuration of the reference patch, reference md, and proposed DMC antennas and a summary of the design parameters are presented in Table 1.

Next, the resonant frequency of the proposed antenna has been determined and analyzed using equivalent circuit modeling, as displayed in Fig. 4(a). To verify the diverse magnetic resonant currents through the radiator and shorting via at the center frequency, a lumped-element equivalent circuit model has been extracted by a 3-D EM simulation of real and imaginary impedance characteristics. The resonant frequency has been determined by adjusting the vias and offset vias at the end of the antenna radiator and by using a curve fitting method, from which an RLC-equivalent circuit could be extracted, as displayed in Fig. 4(b).

To verify the performance of the beamforming pattern, the proposed DMC antenna elements from Fig. 5. have been configured in 1 × 8 array structures at 5.9 GHz and compared with the conventional patch antenna. The volume of the reference patch arrays (including the ground plane) is $1.1\lambda_0 \times 4.2\lambda_0 \times 0.02\lambda_0$. The proposed DMC antenna array has an identical volume (including the ground plane) of $0.74\lambda_0 \times 3.7\lambda_0 \times 0.02\lambda_0$ for in-vehicle mounting. The beam patterns are shifted through several arbitrary angles until the side-lobe level (SLL) exceeded −10 dB.

The achievable peak scan angles with an SLL of less than −10 dB for the reference patch and proposed DMC arrays are approximately ±45° and ±65°, respectively. Further, for each 3 dB beam coverage with an SLL of less than −10 dB, the angles are approximately ±55° and ±83°, respectively. At a peak angle of ±65° for a typical patch antenna, the gain decreased rapidly as the beam is steered and the sidelobes increases rapidly. For the proposed DMC antenna, the gain variation is only 1.2 dB from the peak gain and the sidelobe varies by more than 10 dB. Moreover, the simulated peak gains for the 1 × 8 reference patch and the proposed DMC antenna were approximately 14.5 and 12.2 dBi, respectively. This is because the total beam pattern characteristics of the array antenna are related to the radiation pattern performance of the single antenna. Therefore, the proposed antenna has a significant advantage in terms of overall antenna size, array antenna beam-steering angle, and gain variation rate, although the peak gain is slightly reduced compared to the conventional patch antenna.

3. Fabrication and measurement

3.1. Measurement of the single antenna

The proposed DMC antenna element has been fabricated by using the parameters summarized in Table 1. To compare the performance of the proposed DMC antenna, reference patch and conventional MD antennas have been also fabricated as well. All the antennas have been fabricated with the same Taconic TLX-9 substrate as indicated in the previous section for simulations. Further, to verify realistic performance, a finite ground size of 1 λ_0 × 1.1 λ_0 × 0.02 λ_0 at 5.9 GHz (corresponding to
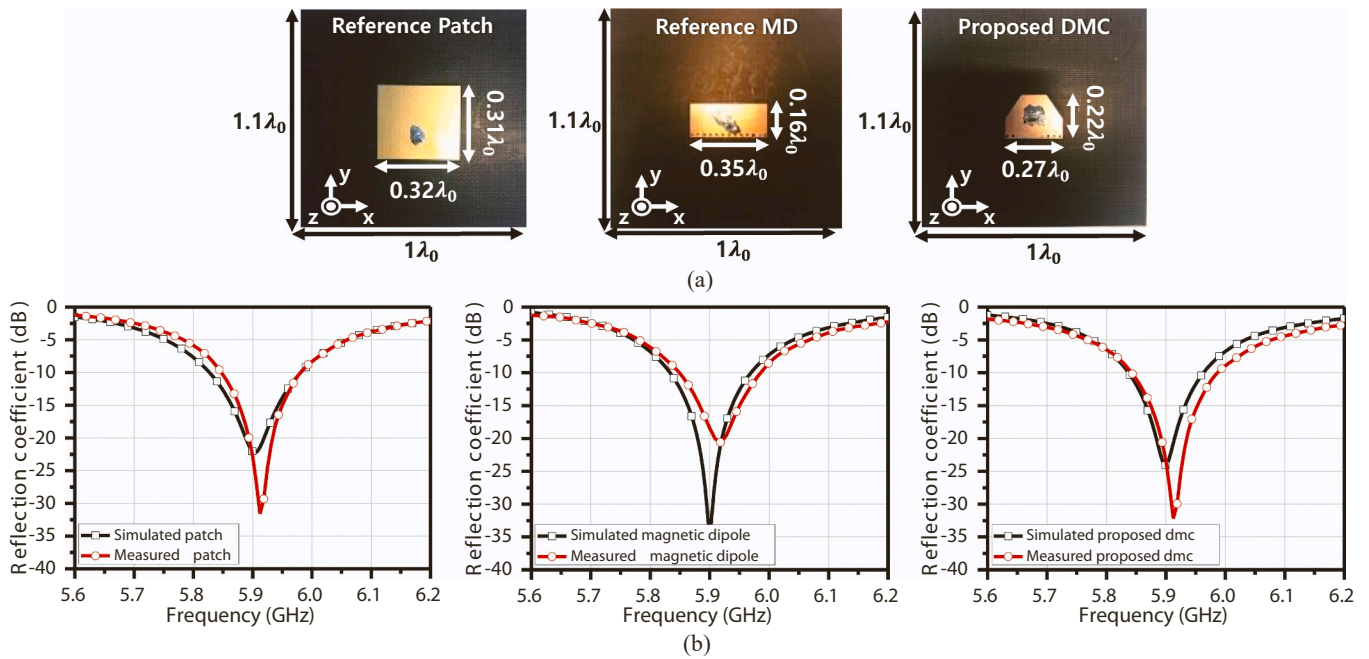
Fig. 6. Implementation of single antennas for (a) reference patch, (b) reference magnetic dipole, (c) proposed DMC, and (d) measured reflection coefficient with total volume of 55 mm × 60 mm × 1.1 mm.
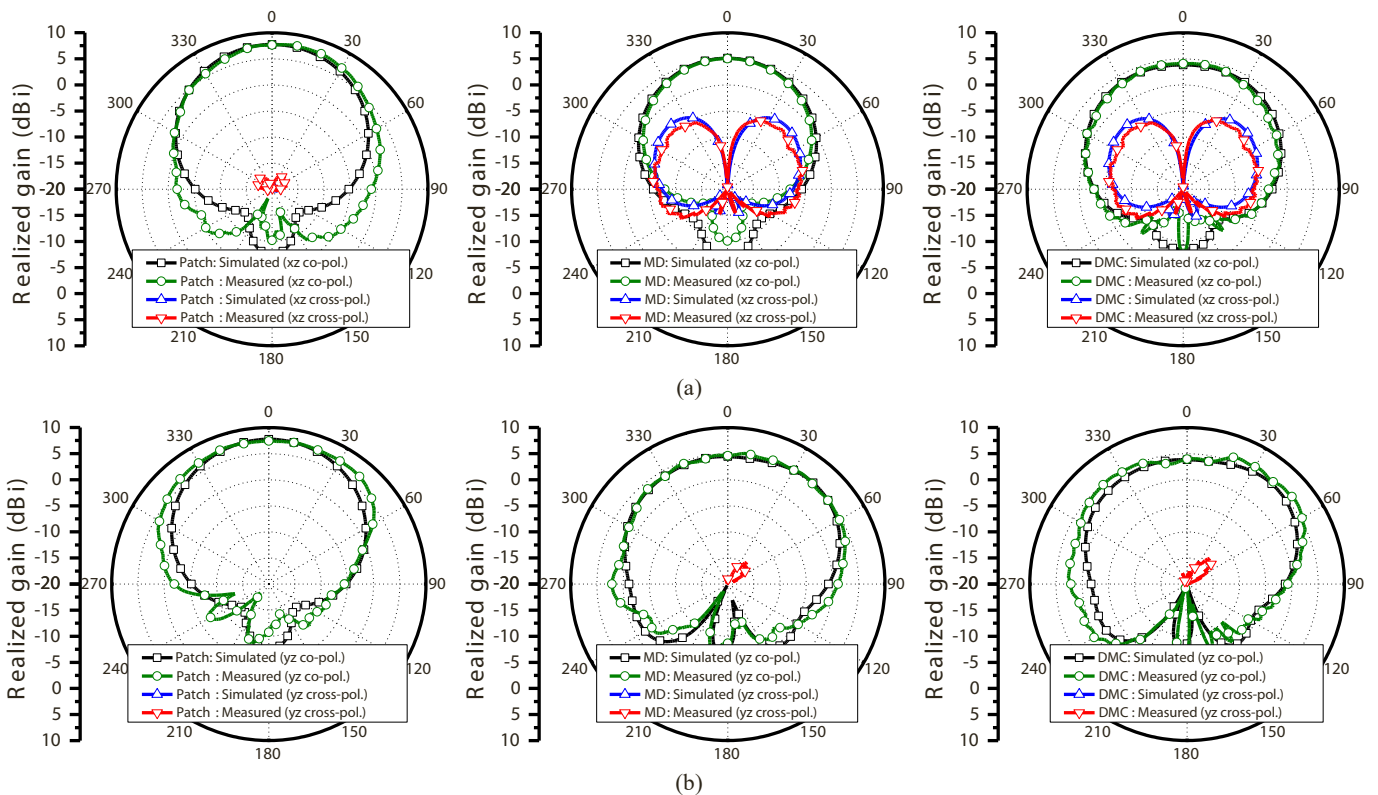

Fig. 7. Measured radiation patterns of the single reference patch, magnetic dipole, and DMC antennas in (a) xz-plane and (b) yz-plane at 5.9 GHz.

55 mm × 60 mm × 1.1 mm) has been used for all the antennas.

Fig. 6(a) displays the fabricated antennas and Fig. 6(b) presents the measured reflection coefficients. The reference patch and MD antennas exhibit 10-dB impedance bandwidths of 180 MHz (5.85–6.03 GHz) and 140 MHz (5.87–6.01 GHz), respectively. In comparison, the proposed DMC antenna exhibits a 10-dB impedance bandwidth of 150 MHz

(5.84–5.99 GHz). Thus, all antennas show good agreement between the simulated and measured reflection coefficients. Then, the radiation patterns have been measured to verify the extended HPBW characteristics of the proposed DMC antenna in both planes, as displayed in Fig. 7.

Fig. 7(a) and (b) depict the radiation patterns of the reference patch, the conventional MD, and the proposed DMC with HPBWs of 71.0°,
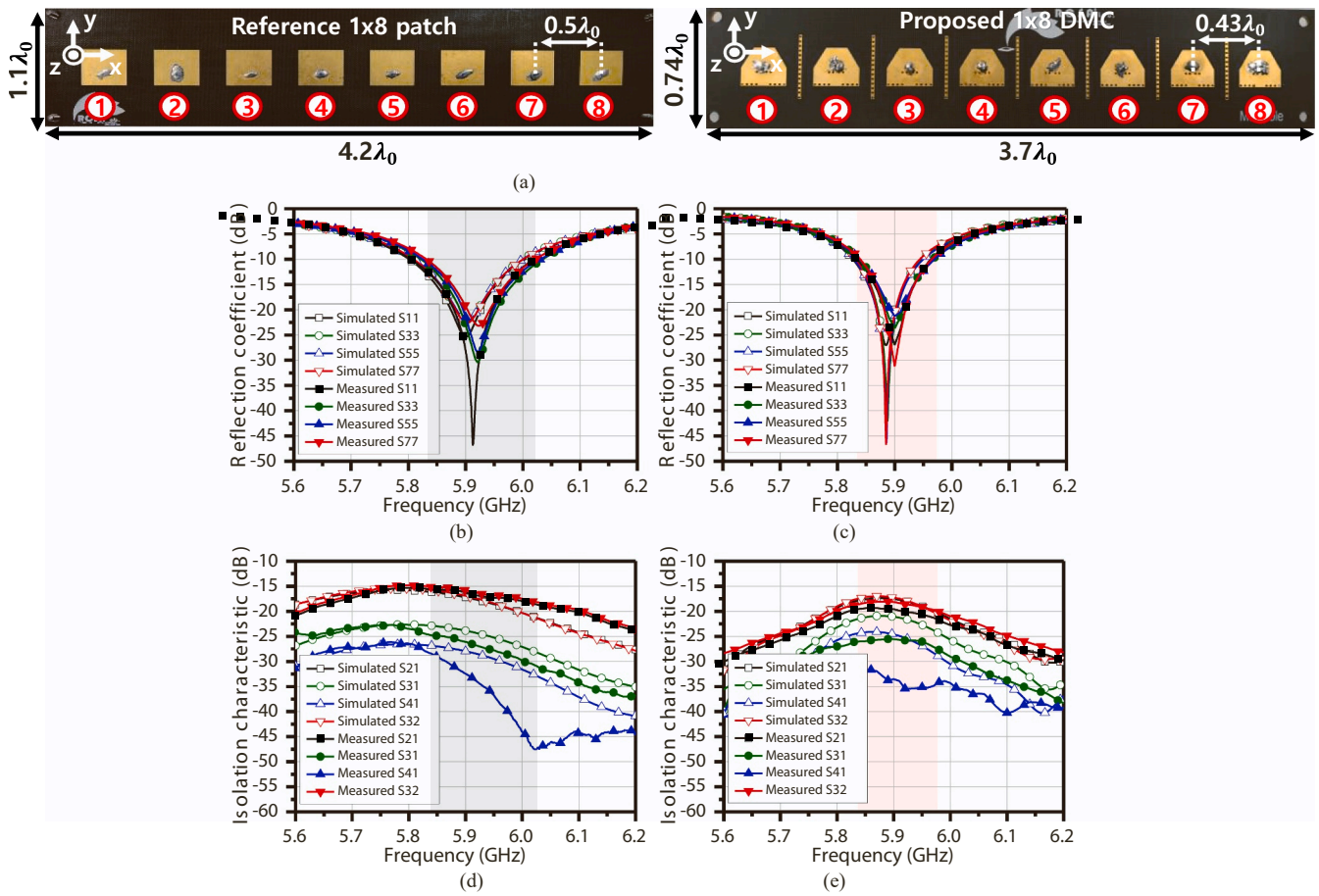
Fig. 8. Fabricated (a) reference patch, proposed DMC arrays, and simulated and measured results for (b)–(c) reflection coefficients and (d)–(e) isolation characteristics of the 1 × 8 reference patch of proposed DMC antennas.

130.0°, and 124° in the xz plane, and HPBWs of 84.7°, 107.7°, and 136° in the yz plane, respectively. Also, the measured peak gains of the reference patch, the conventional MD, and the proposed DMC are 7.6 dBi, 5.5 dBi, and 6.1 dBi, respectively. Thus, the simulations and measurements demonstrate that the proposed single DMC antenna has an extended HPBW in both planes.

3.2. Measurement of the 1-D beam steering antenna module

To verify the extended beam-scanning performance of the proposed DMC antenna, both 1 × 8 reference patch and proposed DMC antenna arrays have been fabricated using the same Taconic TLX-9 substrate. Fig. 8(a) shows the top views of the fabricated reference patch and proposed DMC array antennas with the port numbers. Fig. 8(b) and (c) display the simulated and measured reflection coefficients of the selected antenna ports of the reference and proposed DMC arrays. Here, the 10-dB IBWs of 2.88% (5.84–6.01 GHz) and 2.54% (5.83–5.98 GHz) for the 1 × 8 reference patch and proposed DMC arrays are observed, respectively. Also, Fig. 8(d) and (e) display the measured antenna port-to-port isolation characteristics of the 1 × 8 reference and proposed DMC arrays. The measurements are always better than −15 and −18 dB for the reference and proposed DMC arrays, respectively. Thus, the realized 1 × 8 array configurations exhibit good agreement between the simulated and measured S-parameters.

To drive the phased array operation for the proposed DMC antenna, a 1 × 8 Wilkinson divider and an 8-ch beamformer consisting of commercially available RF phase shifters and attenuators have been also implemented, as displayed in Fig. 9(a). The beamformer has been fabricated with RF-35 Taconic and FR4 substrates forming a four-layer

PCB, as presented in Fig. 9(a). The RF-35 substrate has a relative permittivity of 3.5 and a loss tangent of 0.0018 while the FR4 substrate has a relative permittivity of 4.7 and a loss tangent of 0.018. For the beamformer, 6-bit phase shifters and attenuators having the corresponding resolutions of 5.6° and 0.5 dB, respectively from MACOM Technology Solutions have been adopted. Then, both reference patch and proposed DMC antenna-based phased arrays have been measured in an anechoic chamber to verify the extended beam scanning performance at 5.9 GHz, as displayed in Fig. 9(a). The measured results at 5.9 GHz with de-embedded RF connector and cable losses are displayed in Fig. 9 (b) and (c). The measured HPBW scanning angle of the 1 × 8 patch array satisfying the SLL below −10 dB in the xz plane is 98° (−48° to +50°) while the measured peak gain is 14.7 dBi, as shown in Fig. 9(b). It is observed that the grating lobe of the patch array rises as high as the main lobe at the scanning angle exceeding 100°, proving the limited coverage. In comparison, the measured HPBW scanning angle of the 1 × 8 proposed DMC array satisfying the SLL below −10 dB in the xz plane is 160° (−82° to +78°) while the measured peak gain is 12.7 dBi, as shown in Fig. 9(b). Thus, the scanning coverage is approximately extended by 63% with a small gain variation during the beam-steering. In addition, the antenna elements have been tuned in-phase for the measured beam pattern in the yz-plane, as displayed in Fig. 9(c). The measured HPBW for the proposed DMC array is approximately 132.2°, compared to approximately 71.4° for the patch array in the yz plane. Therefore, the proposed DMC array antenna can cover a wider scan angle in both planes with lower SLL and gain variation.
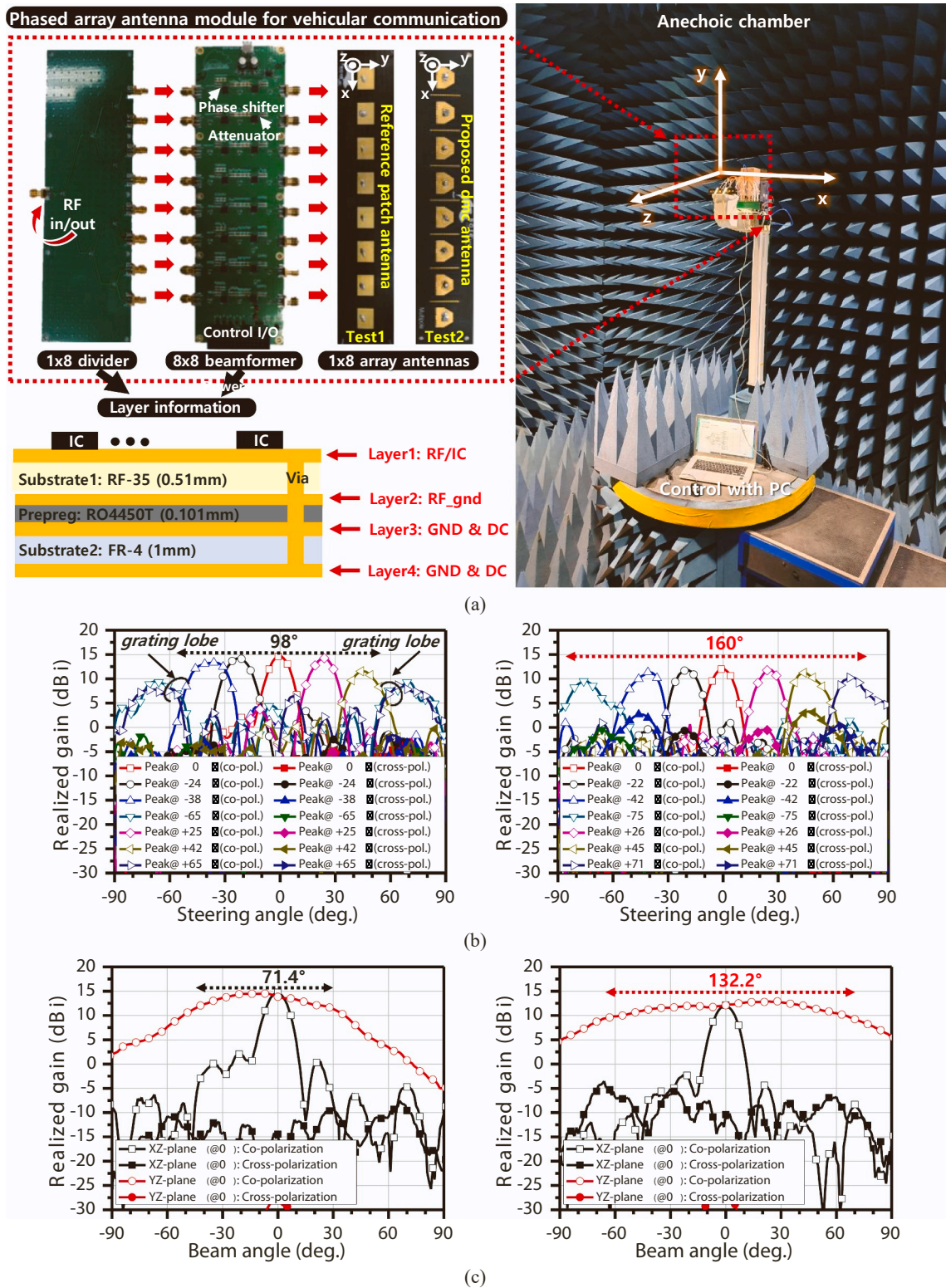
Fig. 9. Proposed phased array antenna module and the measured beamforming pattern: (a) configuration of the beamformer and the measurement test setup, (b) beamforming pattern in xz-plane of reference patch and proposed DMC antenna, and (c) beamforming pattern in xz and yz-planes at in-phase of reference patch and proposed DMC antennas.

3.3. Measurement of the EVM performance

To verify the reference and proposed DMC antennas over-the-air (OTA) in an electromagnetic shielding room, the error vector magnitude (EVM) performance has been verified with NR USRP-2954R 256-QAM signals. Fig. 10 (a) displays the measurement set-up, where an up-converter has been used in the Tx and a down-converter, DC-divider, and hybrid coupler have been used in the Rx. Fig. 10(b) and (c) display the measured EVM values at 28 GHz with 64-QAM and a different position of the Tx horn antenna with Rx beamforming performance. The Tx
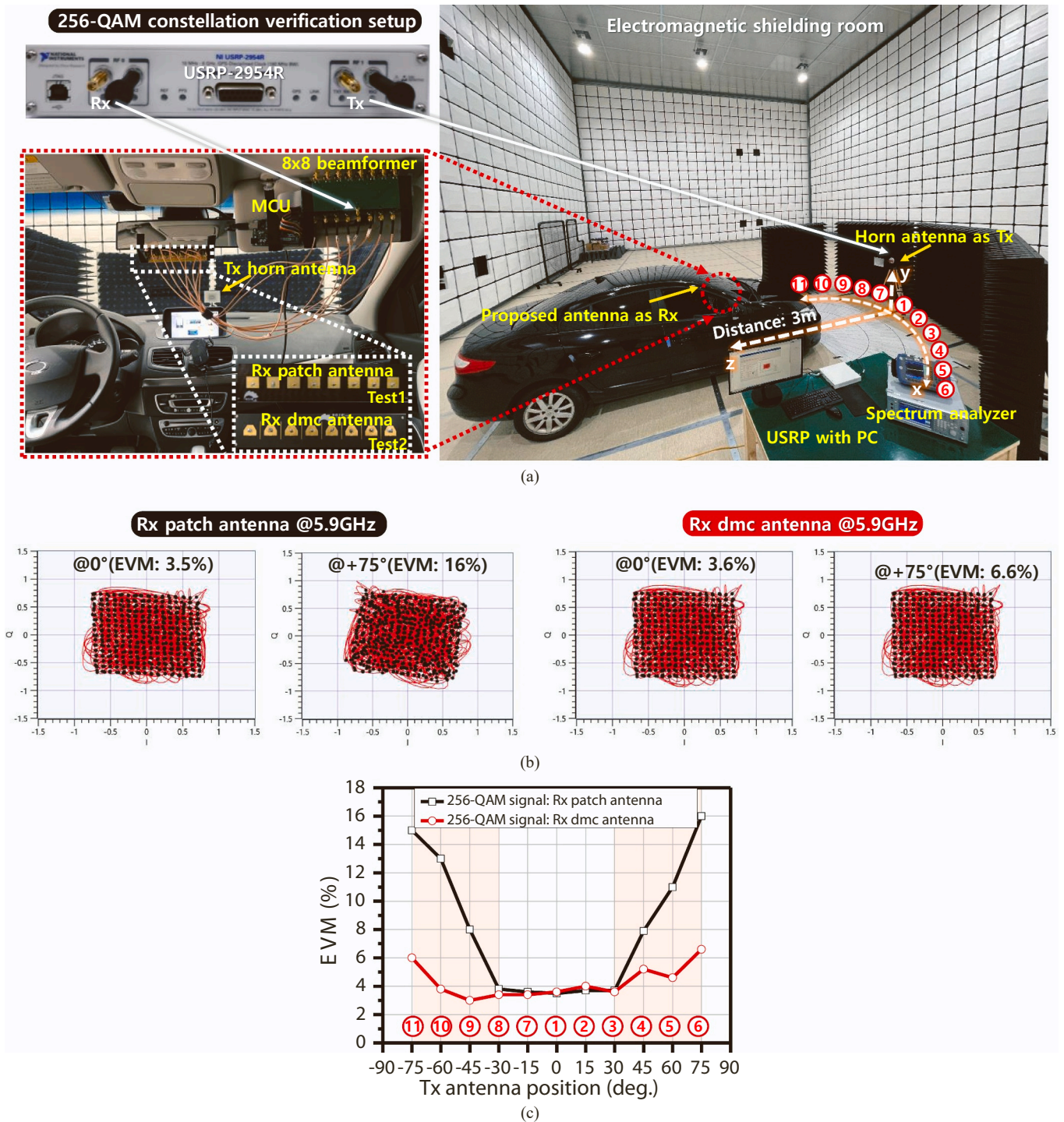
Fig. 10. 256-QAM test of the 1 × 8 reference patch and proposed DMC array antenna: (a) measurement set-up, (b) measured constellations, and (c) measured EVM results at different Tx positions.

Table 2
summary of proposed antenna and its performance comparison with state-of-the-Art Wide beam coverage.

Ref.	Array size	Total volume w/ ground plane	Center Freq. (GHz)	Min. 10-dB BW (%)	Peak gain (dBi)	Aperture eff. @ 0 / 75° (%)	3-dB coverage scan angle (°)	256-QAM EVM @ 75° (%)
[31]	1 × 9	$1.5\lambda_0 \times 4.81\lambda_0 \times 0.03\lambda_0$	5.8	4.4	12.3	13 / 8	154	N/A
[32]	1 × 9	$1\lambda_0 \times 4.81\lambda_0 \times 0.05\lambda_0$	5.8	2.54	12.5	20 / 15	150	N/A
[34]	1 × 8	$1\lambda_0 \times 4.25\lambda_0 \times 0.02\lambda_0$	5.9	2.06	10.8	23 / 18	160	N/A
[37]	1 × 8	$0.67\lambda_0 \times 4.2\lambda_0 \times 0.03\lambda_0$	5.0	18.2	15	42 / 25	120	N/A
This work	1 × 8	$0.74\lambda_0 \times 3.7\lambda_0 \times 0.02\lambda_0$	5.9	2.37	12.7	37 / 31	160	6.6

output power has been set to −27.3 dBm and the Tx horn antenna gain has been set to approximately 20 dBi at 5.9 GHz. The distance between the Tx and Rx antennas has been set to 3 m in the test. The worst EVMs of the Rx reference and DMC antennas are 23.6% and 6.1%, respectively. The proposed DMC antenna demonstrates good EVM measurement results at all positions of the Tx horn antenna compared to the reference patch antenna.

The overall performance of the proposed DMC array antenna is then compared with the other compact wide-beamwidth antennas, as summarized in Table 2. Given the proposed antenna's superior wide-angle performance, the aperture efficiencies of the proposed array with respect to the steered beams at 0° and 75° elevation angles show excellent results. The proposed antenna demonstrates low variation in aperture efficiency across a wide range of angles, whereas the other antennas exhibit either low efficiency or significant degradation from their peak aperture efficiency.

4. Conclusion

In this paper, a new DMC single and array antenna structure have been proposed and compared with the conventional patch single and array antennas. The proposed antenna in a single 1-D array configuration has been verified at 5.9 GHz for wide beamwidth and scanning beam coverage. The proposed antenna has exhibited an excellent wide-angle beamforming performance with low gain variations at different beam steering angles and stable EVM characteristics in any position with a 256-QAM test signal. The measured 3-dB coverage scan angle of the proposed phased array antenna has been 160° while the measured EVM has been 6.6% at 75° incident signal angle. Accordingly, it is expected to be a good candidate for V2X communications using phased array architecture.

Declaration of Competing Interest

The authors declare that they have no known competing financial interests or personal relationships that could have appeared to influence the work reported in this paper.

Acknowledgment

References

[1] E.G. Strom, On medium access and physical layer standards for cooperative intelligent transport systems in Europe, Proc. IEEE 99 (7) () (2011) 1183–1188.

[2] J.B. Kenney, Dedicated short-range communications (DSRC) standards in the United States, Proc. IEEE 99 (7) () (2011) 1162–1182.

[3] K. Sehla, T.M.T. Nguyen, G. Pujolle, P.B. Velloso, Resource allocation modes in C-V2X: from LTE-V2X to 5G-V2X, IEEE Internet Things J. 9 (11) (2022) 8291–8314.

[4] T. Mondal, et al., Vehicular radio scanner using phased array antenna for dedicated Short range communication service, J. Electromagn. Anal. Appl. 4 (9) (2012) 326–366.

[5] R. He, A.F. Molisch, F. Tufvesson, Z. Zhong, B. Ai, T. Zhang, Vehicle-to-vehicle propagation models with large vehicle obstructions, IEEE Trans. Intell. Transp. Syst. 15 (5) (2014) 2237–2248.

[6] M.C. Tan, M. Li, Q.H. Abbasi, M.A. Imran, A wideband beamforming antenna array for 802.11ac and 4.9 GHz in modern transportation market, IEEE Trans. Veh. Technol. 69 (3) (2020) 2659–2670.

[7] D. Manteuffel, "Characteristic Mode based antenna design — A Straight Forward Approach to Small Form Factor Antenna Integration," 2015 9th European Conference on Antennas and Propagation (EuCAP), Lisbon, Portugal (2015) 1-5.

[8] B. Derat, M. Celik, W. Simon and A. Lauer, "Evaluation of Integrated Antenna Performance through Combined Use of Measurement and Full-Wave Simulation," 2020 Antenna Measurement Techniques Association Symposium (AMTA), Newport, RI, USA, (2020) 1-5.

[9] T. Mondal, S. Maity, R. Ghatak, S.R.B. Chaudhuri, Compact circularly polarized wide-beamwidth fern-fractal-shaped microstrip antenna for vehicular communication, IEEE Trans. Veh. Technol. 67 (6) (2018) 5126–5134.

[10] A. Kapoor, P. Kumar, R. Mishra, High gain modified Vivaldi vehicular antenna for Iov communications in 5G network, Heliyon 8 (5) (2020) E09336.

[11] S. Virothu, M. Satya Anuradha, Flexible CP diversity antenna for 5G cellular vehicle-to-everything applications, AEU Int. J. Electron. Commun. 152 (2022) 154248.

[12] E. Abdul-Rahman, D.N. Aloi, Design of a 5G Sub-6 GHz vehicular cellular antenna element with consistent radiation pattern using characteristic mode analysis, Sensors 22 (22) (2022) 8862.

[13] P. Jin, R.W. Ziolkowski, Metamaterial-inspired, electrically small Huygens sources, IEEE Antennas Wirel. Propag. Lett. 9 (2010) 501–505.

[14] M.-C. Tang, Z. Wu, T. Shi, R.W. Ziolkowski, Dual-band, linearly polarized, electrically small Huygens dipole antennas, IEEE Trans. Antennas Propag. 67 (1) (2019) 37–47.

[15] Z. Wu, M.-C. Tang, T. Shi, R.W. Ziolkowski, Two-port, dual-circularly polarized, low-profile broadside-radiating electrically small Huygens dipole antenna, IEEE Trans. Antennas Propag. 69 (1) (2021) 514–519.

[16] W. Lin, R.W. Ziolkowski, Electrically small, single-substrate Huygens dipole rectenna for Ultracompact wireless power transfer applications, IEEE Trans. Antennas Propag. 69 (2) (2021) 1130–1134.

[17] Z. Wu, M.-C. Tang, R.W. Ziolkowski, Broadside radiating, low-profile, electrically small, Huygens dipole Filtenna, IEEE, Antennas Wirel. Propag. Lett. 21 (3) (2022) 556–560.

[18] Y. Yu, Z. Qi, D. Yi, M.-C. Tang, R.W. Ziolkowski, Miniaturized and highly sensitive epidermal Rfid sensor for reliable skin temperature monitoring at a distance, IEEE Sens. J. 3 (6) (2023) 5757–5765.

[19] W. Yang, L. Gu, W. Che, Q. Meng, Q. Xue, C. Wan, A novel steerable dual-beam metasurface antenna based on controllable feeding mechanism, IEEE Trans. Antennas Propag. 67 (2) (2019) 784–793.

[20] T. Li, Z.N. Chen, Compact wideband wide-angle polarization-free metasurface lens antenna array for multibeam base stations, IEEE Trans. Antennas Propag. 68 (3) (2020) 1378–1388.

[21] B. Xi, Y. Xiao, M. Li, Y. Li, H. Sun, Z. Chen, Wide-angle scanning phased array antennas using metasurface slabs, IEEE Trans. Antennas Propag. 69 (12) (2021) 9003–9008.

[22] A.M. Hakimi, A. Keivaan, H. Oraizi, A. Amini, Wide-scanning circularly polarized reflector-based modulated metasurface antenna enabled by a broadband polarizer, IEEE Trans. Antennas Propag. 70 (1) (2022) 84–96.

[23] M.S. Rabbani, J. Churm, A.P. Feresidis, Continuous beam-steering low-loss millimeter-wave antenna based on a piezo-electrically actuated metasurface, IEEE Trans. Antennas Propag. 70 (4) (2022) 2439–2449.

[24] Z. Wang, Y. Dong, Z. Peng, W. Hong, Hybrid metasurface, dielectric resonator, low-cost, wide-angle beam-scanning antenna for 5g base station application, IEEE Trans. Antennas Propag. 70 (9) (2022) 7646–7658.

[25] Y.J. Cheng, W. Hong, K. Wu, Millimeter-wave half mode substrate integrated waveguide frequency scanning antenna with quadri-polarization, IEEE Trans. Antennas Propag. 58 (6) (2010) 1848–1855.

[26] K. Gong, Z.N. Chen, X. Qing, P. Chen, W. Hong, Substrate integrated waveguide cavity-backed wide slot antenna for 60-Ghz bands, IEEE Trans. Antennas Propag. vol. 60 (12) (Dec. 2012) 6023–6026.

[27] W. Han, F. Yang, J. Ouyang, P. Yang, Low-cost wideband and high-gain slotted cavity antenna using high-order modes for millimeter-wave application, IEEE Trans. Antennas Propag. 63 (11) (2015), 4624–463.

[28] J.-W. Kim, H.-W. Jo, K.-S. Kim, G. Kim, S.-C. Chae, J.-W. Yu, Gain Enhanced wide azimuth beam antenna using half-mode substrate integrated waveguide cavity for automotive rear-view mirror application, IEEE Trans. Veh. Technol. 71 (1) (2022) 33–40.

[29] D. René-Loxq, O. Lafond, M. Himdi, L. Roy, F. Ghaffar, Reconfigurable half-mode siw antenna using uniaxial field programmable microwave substrate structure, IEEE Trans. Antennas Propaga. 70 (11) (2022) 11103–11108.

[30] A.H. Murshed, et al., A half-mode cavity backed hybrid array antenna using substrate integrated waveguide (SIW) technology, IEEE Trans. Antennas Propaga. 71 (1) (2023) 169–179.

[31] C.-M. Liu, S.-Q. Xiao, H.-L. Tu, Z. Ding, Wide-angle scanning low profile phased array antenna based on a novel magnetic dipole, IEEE Trans. Antennas Propag. 65 (3) (2017) 1151–1162.

[32] C.-M. Liu, S. Xiao, X.-L. Zhang, A compact, low-profile wire antenna applied to wide-angle scanning phased array, IEEE, Antennas Wirel. Propag. Lett. 17 (3) (2018) 389–392.

[33] Y.-B. Kim, H.-J. Dong, K.-S. Kim, H.L. Lee, Compact planar multipole antenna for scalable wide beamwidth and bandwidth characteristics, IEEE Trans. Antennas Propag. 68 (5) (2020) 3433–3442.

[34] Y.-B. Kim, S. Lim, H.L. Lee, Electrically conformal antenna array with planar multipole structure for 2-D Wide angle beam steering, IEEE Access 8 (2020) 157261–157269.

[35] H. Yang, X. Cao, J. Gao, H. Yang, T. Li, A wide-beam antenna for wide-angle scanning linear phased arrays, IEEE, Antennas Wirel. Propag. Lett. 19 (12) (2020) 2122–2126.

[36] W.-H. Zhang, Q. Xue, S. Liao, W. Che, W. Yang, Low-profile compact microstrip magnetic dipole antenna with large beamwidth and broad bandwidth for vehicular applications, IEEE Trans. Veh. Technol. 70 (6) (2021) 5445–5456.

[37] Y.-F. Cheng, Y.-X. Wang, J. Feng, J.-L. Zhong, C. Liao, X. Ding, A simple wide-angular scanning phased array with wideband filtering response, IEEE Trans. Antennas Propag. 70 (9) (2022) 7703–7712.